Appl Phys B (2008) 93: 507–513
DOI 10.1007/s00340-008-3197-x

Applied Physics B
Lasers and Optics

Optical field dynamics in a wavelength-versatile, all-solid-state intracavity cascaded pulsed Raman laser

H.M. Pask · R.P. Mildren · J.A. Piper

Received: 20 May 2008 / Published online: 17 September 2008

Abstract Monitoring the optical field energies in an intracavity cascaded crystalline pulsed Raman laser enables us to probe the dynamics and optimise the performance of the laser, which produces up to 2.1 W average output power at 4 wavelengths between 532 and 636 nm selectable by simple angle tuning.

PACS 42.55.Ye · 42.72

1 Introduction

Intracavity stimulated Raman shifting (SRS) of Nd lasers in crystalline media, combined with sum frequency generation (SFG), offers a practical and efficient means of generating laser output in the yellow–orange spectral region, which is not readily accessed by conventional solid-state lasers. This spectral region is of increasing interest for applications including biomedical diagnostics and therapy, remote sensing and visual display, and a diversity of laser sources operating at these wavelengths have been reported recently including frequency-doubled Yb fibre lasers [1, 2], direct nonlinear sum-frequency-mixing of the 1.06 and 1.32 μm lines of two Nd:YAG lasers [3, 4], and optically-pumped, frequency-doubled semiconductor Vertical Cavity Surface Emitting Lasers [5, 6]. Wavelength-selectable intracavity frequency-doubled Raman lasers have delivered average powers up to 1.8 W in the yellow–orange spectral region, with diode-visible conversion efficiencies up to 8% [7]. The simplicity and compactness of frequency-doubled Raman lasers, based on well-established all solid-state Nd laser technology, makes them very attractive sources in the yellow–orange.

Recently [8], we reported that the cascaded nature of the SRS process can be utilised to generate wavelength-selectable output at visible wavelengths spanning the green–yellow–red spectrum, and the scheme has also been recently adopted for wavelength-selectable Raman laser operation in the ultraviolet [9]. In an Nd-based intracavity Raman laser, the fundamental optical field at 1064 nm is cavity-dumped through the nonlinear process of SRS (resonator mirrors are chosen to provide high Q at the fundamental). Given sufficiently-broad mirror coatings, the fundamental, first, second and potentially higher-order Stokes wavelengths can all be resonated. It is this "cascading" nature of the SRS process which enables generation of wavelength-selectable output in the visible, achieved by means of configuring a nonlinear crystal to frequency double the fundamental, or the first Stokes, or the second Stokes and so on. Alternatively, the nonlinear crystal can be configured to generate the sum frequency of these wavelengths. The basic scheme is depicted in Fig. 1, showing the energy flow between the various optical fields. Also shown are the wavelengths obtainable from the various sum frequency combinations of the fundamental and the first two Stokes orders from $KGd(WO_4)_2$ (KGW). Suitable choices for the nonlinear media are LBO (angle or temperature tuned) or BBO (angle-tuned). The key challenge is to design the laser resonator so that the various processes of generating laser emission at the fundamental, frequency conversion through the SRS process and frequency doubling/mixing, are simultaneously optimised.

H.M. Pask (✉) · R.P. Mildren · J.A. Piper
MQ Photonics, Macquarie University, Sydney, NSW 2109, Australia
e-mail: hpask@ics.mq.edu.au
Fax: +61-2-98508983

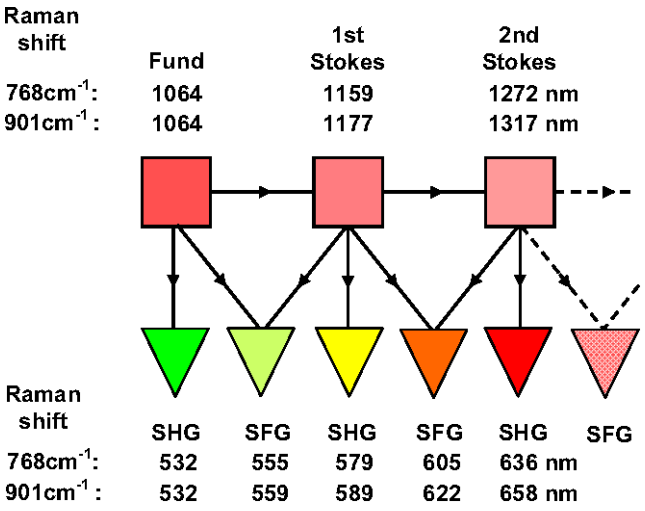

Fig. 1 Schematic diagram showing the interaction of the fundamental optical field at 1064 nm, the first and second Stokes optical fields, and the various visible wavelengths obtained through SHG and SFG when using the two main Raman transitions of KGW

In this paper we describe the performance of a compact (15 cm long) and efficient wavelength-versatile Raman laser based on a Q-switched Nd:YAG laser with intracavity Raman shifting in KGW and intracavity frequency doubling in BBO. Angle-tuning of the BBO enables operation at up to 5 wavelengths across the visible. Experimental data which illustrate the energy transfer dynamics which underpin the wavelength selectability aspect of the laser are presented, and we discuss how these can be used to optimise laser performance.

2 Design and operation the wavelength-versatile laser

The experimental arrangement is shown in Fig. 2. It differs from that reported in [8] in four significant aspects. First, a simple linear configuration incorporating straightforward dichroic short-pass and long-pass mirror coatings is employed, instead of the folded cavity reported previously. Second, BBO is chosen as the frequency doubling crystal as only a few degrees of angle-tuning enables selection of up to 5 discrete wavelengths. LBO was used in [8], and operation was limited to four wavelengths. Third, the KGW is 25 mm long, compared to 50 mm used in [8]; this reduces the length of the resonator and because the optical stability of the resonator at high pump powers is limited by strong thermal lensing in the Nd:YAG, the shorter resonator enables more robust operation of the laser. These three changes enable the laser to operate efficiently at 5 different wavelengths, with improved alignment sensitivity. Finally we also include a plane dichroic intracavity mirror (M3) which directs both the forwards- and backwards-propagating frequency doubled output into a single visible output beam.

The pump source is a fibre-coupled (400 μm, 0.22NA), 808 nm diode laser delivering up to 21 W output power. Two lenses image the output into the Nd:YAG laser crystal (5 mm dia × 5 mm long, 1% doping) with a pump spot size (beam radius) of ∼250 microns. The (flat) pumped face of the Nd:YAG crystal is coated for high reflectivity from 1060–1200 nm, and the (flat) rear surface is AR coated at 1064 nm. The fundamental output (1064 nm) is acousto-optically Q-switched at 5–50 kHz. The laser resonator is ∼15 cm long, defined by the coated plane face (M1) of the Nd:YAG laser crystal and an output coupler with (concave) radius of curvature 200 mm (M2). The output coupler is coated to provide high transmission in the visible (532–650 nm) and high reflectivity in the infrared (1060–1200 nm). Also included in the resonator is the plane intracavity mirror (M3) to direct the backwards propagating visible output into a single forwards propagating output beam. M3 has one side coated for high transmission (>98%) at wavelengths greater than 1060 nm, and high reflectivity for wavelengths shorter than 750 nm. The other side of the mirror was an AR-coated (1060–1200 nm). The separation between the output coupler M2 and the BBO crystal was a critical parameter in optimizing the conversion efficiency to the visible.

A KGW crystal (EKSMA, 5 × 5 × 25 mm, cut for propagation along the optical N_p-axis and oriented so that its N_m-axis was in the vertical plane) was chosen as the Raman medium, as KGW offers high optical damage threshold, good thermal properties and fairly high Raman gain for Raman shifts of 768 and 901 cm^{-1} [10]. The Raman gain is polarisation-dependent, so that for fundamental light polarised parallel to the N_m-axis, a Raman mode with Stokes

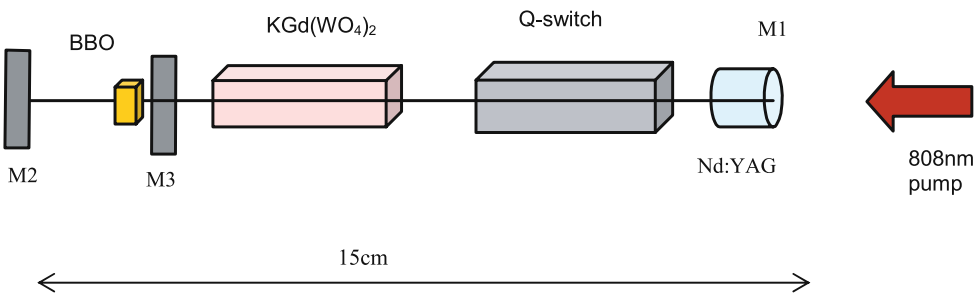

Fig. 2 Experimental arrangement for the wavelength-versatile Raman laser

Table 1 Output wavelengths, corresponding phasematching angle and output power achieved for phasematching in (a) the horizontal plane and (b) the vertical plane. 17 W diode power, 12 kHz prf

Output wavelength	532 nm	555 nm	579 nm	605 nm	636 nm
Output power	1.7 W	0.50 W	1.1 W	0.28 W	0.04 W
BBO angle [11]	22.8°	22.2°	21.7°	21.1°	20.7°
Output wavelength	532 nm	559 nm	588 nm	621 nm	658 nm
Output power	2.1 W	0.77 W	1.2 W	0.07 W	–
BBO angle [11]	22.8°	22.1°	21.5°	20.9°	20.4°

shift of 901 cm^{-1} has highest Raman gain, while for fundamental light polarised parallel to the N_g-axis, the Raman gain is highest for the 768 cm^{-1} Stokes shift. The laser was operated without a polariser because it was found that even two Brewster plates were insufficient to constrain laser oscillation to a single polarisation in the high-Q resonator and large losses at the Brewster plates made the laser inefficient. However the phase matching conditions of the frequency doubling/summation effectively results in selection of only one polarisation mode at any one time.

Second harmonic/sum frequency generation was achieved using a BBO crystal (Castech, $4 \times 4 \times 4$ mm) cut for type I critical phase-matching, AR coated at 1060–1200 nm, and placed close to the intracavity mirror, near the beam waist. When the BBO crystal was oriented for phasematching in the horizontal plane, which contained the optical N_m-axis of the KGW crystal, the 768 cm^{-1} Raman shift determined the output wavelengths. When the BBO was oriented for phasematching in the vertical plane, containing the N_g-axis of the KGW crystal, the 901 cm^{-1} shift determined the output wavelength.

3 Laser output characteristics

The laser performance was investigated for both 768 and 901 cm^{-1} Raman shifts, i.e. for phasematching in the horizontal and vertical planes, respectively. In each case, the laser was operated with 17 W diode pump power incident on the Nd:YAG crystal, Q-switched at 12 kHz prf, and optimised for maximum output power at 588 or 579 nm. For a given planar orientation, only the phasematching angle of the BBO need be adjusted to generate the set of visible wavelengths associated with a particular Raman mode, though some minor adjustment of the cavity end-mirror was often needed to maximise output. The output powers achieved at each wavelength and the calculated phasematching angles for each wavelength [10] are shown in Table 1, for the two cases of phasematching in the vertical and horizontal planes.

The laser output typically contained some infrared output that was transmitted through the end mirror (M2) in addition to the laser output at the selectable visible wavelength. This was less than 50 mW when the conversion efficiency

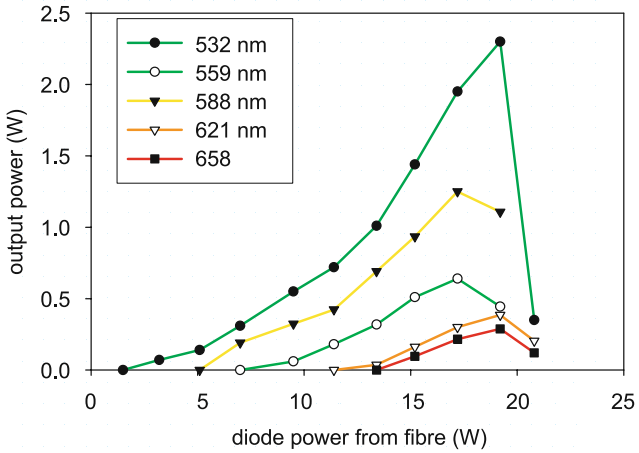

Fig. 3 Laser output characteristics at selected visible wavelengths. 12 kHz pulse repetition frequency

to the visible was high. On the other hand, output powers up to 380 mW (mostly at the second Stokes wavelength) were observed when the BBO crystal was unphasematched. A selection of filters was used to separate the infrared and visible components.

Up to five visible outputs could be selected, compared with only three in the case of angle-tuned LBO and four in the case of temperature-tuned LBO [8]. This is a result of the more-favourable phasematching properties of BBO over the wavelength range of interest. All 5 wavelengths can be obtained using BBO for a rotation of <3 degrees, whereas LBO (cut to phasematch 1158/579 nm) required a rotation of 17 degrees to select between 3 wavelengths, and the BBAR coatings (optimised for normal incidence) became substantially less effective. Temperature tuning of LBO using dual crystals to phasematch over the required wavelength range has advantages of simple non-mechanical control but introduces significantly higher intracavity losses with lowers conversion efficiency [8].

In Fig. 3, output powers at 532, 559, 588, 605 and 658 nm are shown as a function of input power from the laser diode. For these results, the laser was Q-switched at 13 kHz and the resonator aligned to obtain maximum output at each selected wavelength. The spectral purity of the visible output beam (determined using an Ocean Optics fibre spectrometer) was high: >99% of the output beam was at the selected

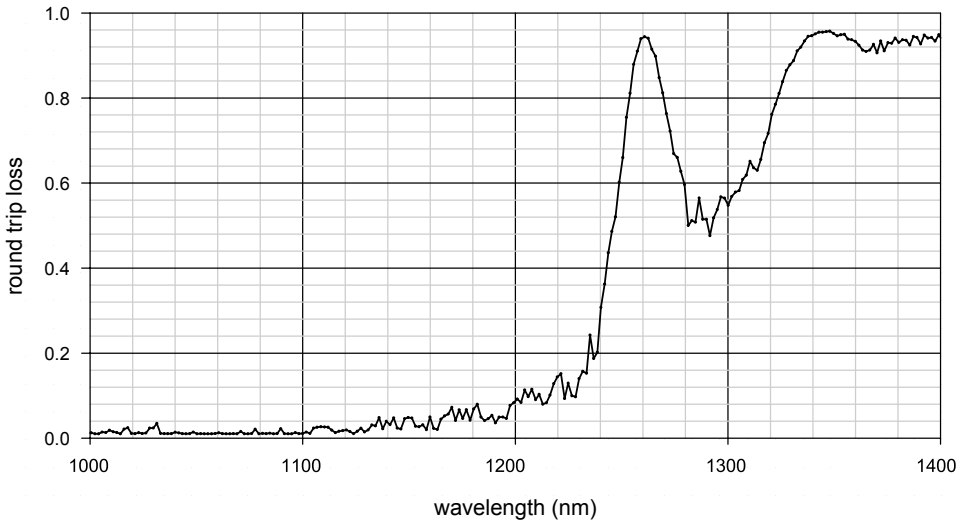

Fig. 4 Experimentally-determined resonator round trip losses as a function of wavelength

wavelengths between 532–588 nm and >95% for selected wavelengths between 605–658 nm.

Lower output powers at wavelengths from 605–658 nm are assumed to be the consequence of large resonator mirror losses for wavelengths longer than 1200 nm. These losses occur mainly at the HR coating on the Nd:YAG crystal and the output coupler M2. It is expected that much higher output powers could be achieved using an Nd:YAG crystal with broadband AR coatings and resonator end mirrors with short-wave pass dichroic coatings to provide transmission at the visible and diode wavelengths, and wider reflectivity band 1064–1320 nm. The transmission characteristics of each resonator component were measured individually and then multiplied to determine the cumulative round trip loss for the resonator as a function of wavelength, as shown in Fig. 4. While the uncertainties in the calculated cumulative losses are quite high (±10%, determined by summing the percentage errors for each transmission measurement), the cumulative round-trip losses at the longer wavelengths (e.g. second Stokes wavelengths) are clearly very substantial compared to the effective loss due to internal frequency conversion, estimated at 10%.

It is apparent from Fig. 3 that there is a rollover in visible laser output for diode pump powers greater than 17 W, above which the thermal lens in the Nd:YAG laser crystal becomes so strong that the resonator approaches the optical stability limit (the resonator also becomes increasingly sensitive to alignment). For output powers 17 W and below, the resonator operated robustly and was easy to align, and the laser gave stable repeatable output.

The optical to optical (diode to visible) conversion efficiencies were up to 7.3% for output at 588 nm and up to 12.2% for output at 532 nm. Comparing with data from our previous report of wavelength-selectable laser operation [8], the diode to 588 nm conversion efficiencies are similar, in spite of the use of a shorter KGW Raman crystal (25 mm cf. 50 mm). While the Raman gain coefficient is proportional to crystal length, the shorter crystal and intracavity mirror afford a shorter resonator (15 cm cf. 25 cm) and greater flexibility in positioning components, thus reducing the resonator mode size and improving the efficiency of the various nonlinear conversion processes. Shorter duration pulses and higher peak powers resulting from the shorter resonator also favour high conversion efficiency. The low threshold for SRS also suggests that it may be possible to work with even shorter KGW crystals, which would be beneficial in enabling even shorter resonators to be used.

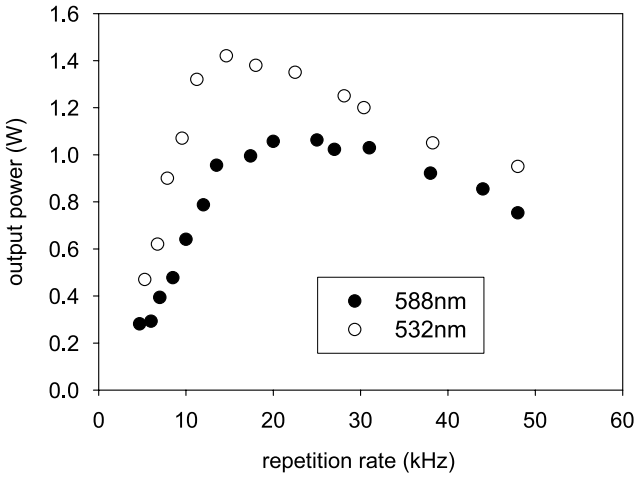

Fig. 5 Laser output power at 532 and 588 nm as a function of pulse repetition frequency

The dependence of laser output power on pulse repetition rate was investigated, and data showing output power for 532 and 588 nm are presented in Fig. 5, for diode pump power ~15 W. There is a clear difference in the optimum repetition rate for the two wavelengths in that the highest

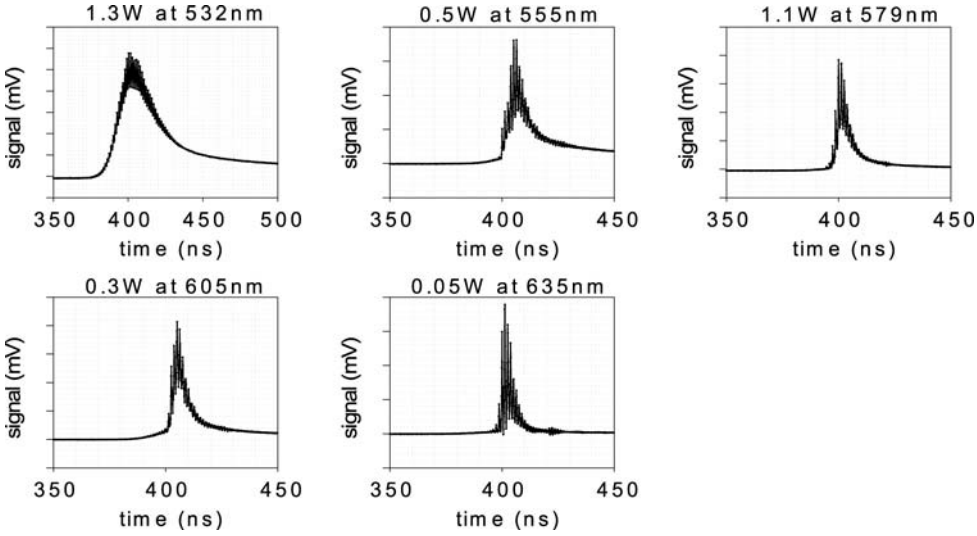

Fig. 6 Typical pulse shapes for selected visible wavelengths (Diode power 15 W, pulse repetition frequency 25 kHz)

output at 532 nm occurs at around 13 kHz, while the maximum output at 588 nm occurs at around 25 kHz. The highest peak powers at the fundamental Nd:YAG transition occur at around 13 kHz, and it is usual for the output power at 532 nm to peak around this value. The average power at 588 nm (frequency-doubled first Stokes) maximises at higher repetition rates since intracavity peak powers are thereby reduced, limiting SRS cascading to higher-order Stokes, while maintaining sufficiently high optical field intensity for efficient frequency doubling. This explanation is supported by the analysis of laser optical fields presented in the following sections.

The temporal profiles for the various visible wavelengths, measured using a 5 GHz photodiode and 2 GHz oscilloscope, are shown in Fig. 6. The pulse duration (full-width at half maximum) is longest at around 50 ns for output at 532 nm, while somewhat shorter pulses (10–20 ns) are obtained for the longer (frequency-doubled Stokes) wavelengths. This is entirely consistent with pulse shortening which is a well-known feature of intracavity Raman lasers [12]. Note that the frequency-doubled Stokes pulses exhibit some modulation, also common in intracavity Raman lasers [12].

Shown in Fig. 7 is the residual fundamental output at 1064 nm, for the two cases where the selected visible wavelengths are 532 or 579 nm. When 532 nm is selected, there is no SRS, and the residual fundamental pulse is broadly similar to the familiar QS pulse obtained in a high-Q cavity, having a long decay time of ∼100 ns. When 579 nm is selected, the residual fundamental pulse shows the initial buildup reflecting rapid energy transfer from the population inversion to the optical field when the Q-switch is opened, followed by rapid depletion, indicative of cavity dumping, once the threshold for SRS is reached.

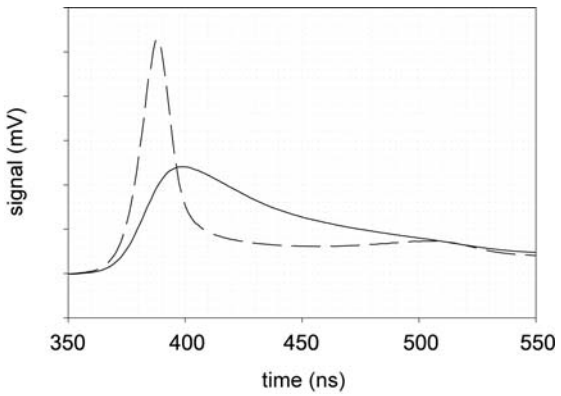

Fig. 7 Residual output at 1064 nm for cases of (a) 1.7 W output at 532 nm (*solid line*) and (b) 1.1 W output power at 579 nm (*dashed line*). Diode wavelength was 17 W, prf 13 kHz

4 Optical field dynamics

In order to probe the dynamics of the cascaded Raman laser, the near-IR spectral content of the laser output was measured for a range of laser operating conditions. The data, in combination with the optical loss characteristics of the resonator, were then used to determine the time-averaged spectral content of the optical fields related to the various fundamental and Stokes waves inside the resonator.

Measurements of optical field energies were made using a fibre-optic spectrometer (Ocean Optics) calibrated using a black body source to ensure flat spectral response. A portion of the laser output was sampled by reflection from a microscope slide positioned at <10 deg angle of incidence. The spectrometer covered the wavelength range ∼900–1700 nm, which enabled the optical field energy to be determined at the fundamental (1064 nm), first Stokes (1158 or 1176 nm) and second Stokes (1273 nm or 1316 nm). The integration time of the detector was set around 50 ms, so that the spec-

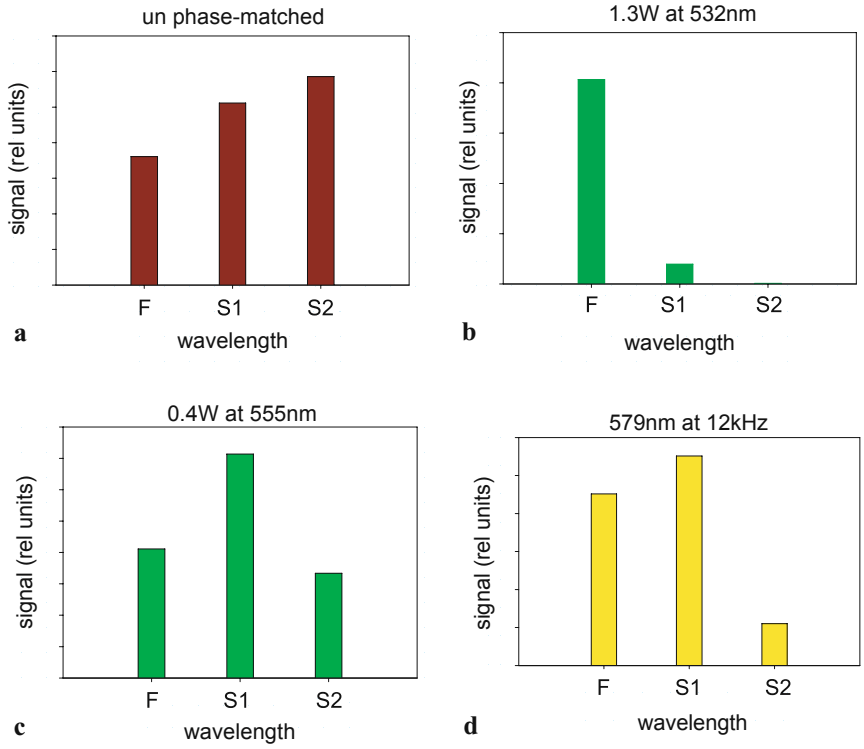

Fig. 8 Experimentally-determined spectral content of the time-averaged intracavity field for various phasematching configurations of BBO: (**a**) not phase-matched for visible generation, and (**b**–**d**) phasematched to generate 532, 555 and 579 nm

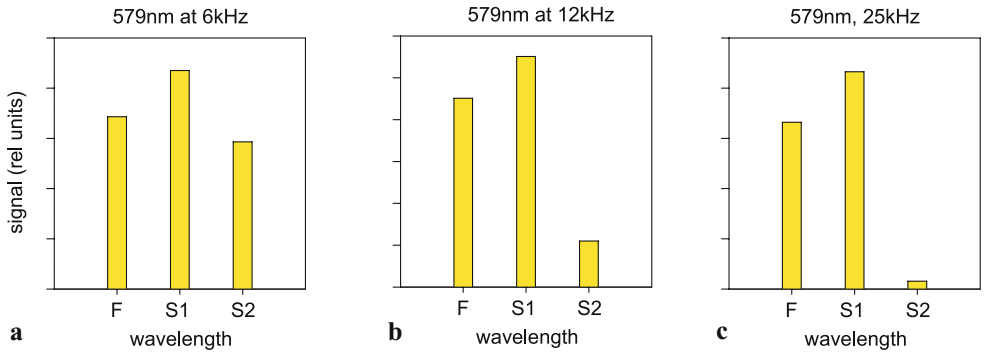

Fig. 9 Experimentally-determined spectral content of the time-averaged intracavity field when BBO was phase-matched to generate 579 nm and the pulse repetition frequency was (**a**) 6 kHz, (**b**) 12 kHz and (**c**) 25 kHz

tral content was averaged over many pulses. A polariser and an optical filter were used to prevent any visible light from entering the spectrometer.

The spectral bandwidth of the spectrometer (∼2 nm) was substantially broader than the linewidth of the various infrared lines of interest. The actual linewidths were measured using an Optical Spectrum Analyser to be <0.15 nm (instrument limited). The relative energy at the fundamental and Stokes wavelengths was determined from the area under the (calibrated) peaks in the detector signal from the spectrometer. This approach was validated by comparing the results to the output powers at the various wavelengths measured using a power meter (Ophir) and various optical filters.

To estimate the relative spectral content of the optical fields inside the laser cavity, it was necessary to consider the fraction of the intracavity power which exited the cavity through the output coupler (as opposed to through the input mirror or by other means). This is given by the ratio of the output coupler transmission and the round trip resonator losses (see Fig. 4), and is different for each wavelength of interest, i.e., the fundamental, first and second Stokes. The spectra recorded after the output coupler were scaled using this ratio, and we were therefore able to make relative measurements of the time-averaged fundamental and Stokes intracavity optical fields. The purpose of these experiments was to provide a qualitative picture of the interacting optical fields when different visible wavelengths were selected. The shot to shot variations between spectra were typically 10–20%.

In Fig. 8, the spectral content of the time-averaged intracavity field is shown, for the cases of phasematching (in the horizontal plane) for SHG (532, 579 nm), and SFG (559 nm) and also when the BBO crystal was oriented to avoid phasematching at these wavelengths. Data was recorded for a

diode pump power of 17 W and pulse repetition rate of 12 kHz. When the BBO crystal was not phasematched, the cascaded SRS process was such that the intracavity energy was distributed between the fundamental, first and second Stokes optical fields as shown by the bars in Fig. 8(a). No third Stokes signal was observed at any time as a result of the high resonator losses at wavelengths >1350 nm. When the BBO was rotated to phasematch the 1064/532 nm interaction, producing 1.3 W at 532 nm, the intracavity energy was almost all confined to the fundamental; a small amount of energy resided in the first Stokes optical field, and there was no second Stokes (see Fig. 8(b)). When 555 and 579 nm were selected, the optical field energies were distributed as shown in Figs. 8(c) and (d). Of particular note is the almost total absence of energy in the second Stokes optical field when 579 nm is selected, as strong depletion of the first Stokes field via the SHG process inhibits second Stokes generation.

Monitoring the spectral content of the intracavity fields for different configurations of the nonlinear crystal (and therefore different visible output wavelengths) provides a convenient tool which enables us to optimise laser performance for particular visible outputs. The spectral content depends both on resonator design parameters (resonator length, mirror curvatures and thermal lensing, which determine resonator mode-sizes and mirror coating characteristics) and input/output power settings, including pulse repetition frequency. Figure 9 shows how varying the pulse repetition frequency affects the energy distribution between the infrared optical fields for the cases where the BBO crystal phasematched to produce output at 579 nm. Operation at 6 kHz produces the highest peak powers, and this results in higher energy content in the second Stokes optical field compared to operation at 12 or 25 kHz. When the BBO is phasematched to produce output at 579 nm for a prf of 6 kHz, there is still a high proportion (20%) of energy at the second Stokes wavelength. At 12 kHz this is reduced (9%), while at 25 kHz the second Stokes generation is barely above threshold. These observations provide a qualitative understanding of why the output power at 588 nm optimises for repetition rates around 25 kHz. Another means of minimising energy losses to unwanted higher Stokes orders would be by increasing the nonlinear coupling coefficient for harmonic mixing, for example by optimising the waist sizes in the nonlinear crystal, the nonlinear crystal parameters and the choice of nonlinear material.

5 Conclusions

We have demonstrated an all-solid-state pulsed Raman laser with wavelength-selectable output at up to 5 visible wavelengths, with output powers and efficiencies up to 2.1 W and 12% for output at 532 nm and 1.2 W and 8% at 588 nm, respectively. Maximum output power and optical conversion efficiency of the device are presently limited by strong thermal lensing in the Nd:YAG laser crystal. For the orange–red output, powers are limited by rapidly increasing transmission losses of the mirrors at wavelengths above 1200 nm, and significant improvements in performance are expected with improved mirror coatings.

We have performed relative measurements of the time-averaged intracavity fundamental and Stokes optical fields. These provide qualitative insight into the optical field dynamics and are very useful for optimising laser performance at selected visible wavelengths. Future studies of the dynamics involving numerical modelling combined with temporally-resolved measurements of the fundamental and Stokes fields are planned for the future.

Acknowledgements This research was supported under Australian Research Council's *Discovery Projects* funding scheme.

References

1. S.C. Sinha, C. Langrock, M.J.F. Digonnet, M.M. Fejer, R.L. Byer, Efficient yellow-light generation by frequency doubling a narrow-linewidth 1150 nm ytterbium fiber oscillator. Opt. Lett. **31**(3), 347–349 (2006)
2. D. Georgiev, V.P. Gapontsev, A.G. Dronov, M.Y. Vyatkin, A.B. Rulkov, S.V. Popov, J.R. Taylor, Watts-level frequency doubling of a narrow line linearly polarized Raman fiber laser to 589 nm. Opt. Express **13**(18), 6772–6776 (2005)
3. Y.F. Chen, S.W. Tsai, Diode-pumped Q-switched Nd:YVO_4 yellow laser with intracavity sum-frequency mixing. Opt. Lett. **27**(6), 397–399 (2002)
4. J. Janousek, S. Johansson, P. Tidemand-Lichtenberg, S. Wang, J. Mortensen, P. Buchhave, F. Laurell, Efficient all solid-state continuous-wave yellow-orange light source. Opt. Express **13**, 1188–1192 (2005)
5. A.C. Tropper, H.D. Foreman, A. Garnache, K.G. Wilcox, S.H. Hoogland, Vertical-external-cavity semiconductor lasers. J. Phys. D Appl. Phys. **37**(9), R75–R85 (2004)
6. J. Chilla, Q.-Z. Shu, H. Zhou, E. Weiss, M. Reed, L. Spinelli, Recent advances in optically pumped semiconductor lasers, in *Proc. SPIE Solid State Lasers XVI: Technology and Devices* (2007)
7. H.M. Pask, J.A. Piper, Efficient all-solid-state yellow laser source producing 1.2 W average power. Opt. Lett. **24**(21), 1490–1492 (1999)
8. R.P. Mildren, H.M. Pask, H. Ogilvy, J.A. Piper, Discretely tunable, all-solid-state laser in the green, yellow, and red. Opt. Lett. **30**(12), 1500–1502 (2005)
9. R.P. Mildren, H. Ogilvy, J.A. Piper, Solid-state Raman laser generating discretely tunable ultraviolet between 266–321 nm. Opt. Lett. **32**, 814–816 (2007)
10. I.V. Mochalov, Laser and nonlinear properties of the potassium gadolinium tungstate laser crystal $KGd(WO_4)_2:Nd^{3+}$ (KGW:Nd). Opt. Eng. **36**, 1660–1669 (1997)
11. SNLO nonlinear optics code available from A.V. Smith, Sandia National Laboratories, Albuquerque, NM 87185-1423
12. H.M. Pask, The design and operation of solid-state Raman lasers. Prog. Quantum Electron. **27**, 3–56 (2003)